J Appl Physiol 129: 1140–1149, 2020.
First published October 15, 2020; doi:10.1152/japplphysiol.00359.2020.

RESEARCH ARTICLE | *Hypoxia*

What hinders pulmonary gas exchange and changes distribution of ventilation in immobilized white rhinoceroses (*Ceratotherium simum*) in lateral recumbency?

Martina Mosing,[1] Andreas D. Waldmann,[2] Muriel Sacks,[1] Peter Buss,[3] Jordyn M. Boesch,[7] Gareth E. Zeiler,[4,5] Giselle Hosgood,[1] Robin D. Gleed,[7] Michele Miller,[6] Leith C. R. Meyer,[5] and Stephan H. Böhm[2]

[1]*School of Veterinary Medicine, College of Science, Health, Engineering and Education, Murdoch University, Perth, Australia;* [2]*Department of Anesthesiology and Intensive Care Medicine, Rostock University Medical Center, Rostock, Germany;* [3]*Veterinary Wildlife Services, South African National Parks, Kruger National Park, Skukuza, South Africa;* [4]*Department of Companion Animal Clinical Studies, Faculty of Veterinary Science, University of Pretoria, Onderstepoort, South Africa;* [5]*Centre for Veterinary Wildlife Studies and Department of Paraclinical Studies, Faculty of Veterinary Science, University of Pretoria, Onderstepoort, South Africa;* [6]*Department of Science and Technology-National Research Foundation Centre of Excellence for Biomedical TB Research, South African Medical Research Council Centre for Tuberculosis Research, Division of Molecular Biology and Human Genetics, Faculty of Medicine and Health Sciences, Stellenbosch University, Cape Town, South Africa; and* [7]*Department of Clinical Sciences, College of Veterinary Medicine, Cornell University, Ithaca, New York*

Submitted 7 May 2020; accepted in final form 4 August 2020

Mosing M, Waldmann AD, Sacks M, Buss P, Boesch JM, Zeiler GE, Hosgood G, Gleed RD, Miller M, Meyer LC, Böhm SH. What hinders pulmonary gas exchange and changes distribution of ventilation in immobilized white rhinoceroses (*Ceratotherium simum*) in lateral recumbency? *J Appl Physiol* 129: 1140–1149, 2020. First published October 15, 2020; doi:10.1152/japplphysiol.00359.2020.—This study used electrical impedance tomography (EIT) measurements of regional ventilation and perfusion to elucidate the reasons for severe gas exchange impairment reported in rhinoceroses during opioid-induced immobilization. EIT values were compared with standard monitoring parameters to establish a new monitoring tool for conservational immobilization and future treatment options. Six male white rhinoceroses were immobilized using etorphine, and EIT ventilation variables, venous admixture, and dead space were measured 30, 40, and 50 min after becoming recumbent in lateral position. Pulmonary perfusion mapping using impedance-enhanced EIT was performed at the end of the study period. The measured impedance (ΔZ) by EIT was compared between pulmonary regions using mixed linear models. Measurements of regional ventilation and perfusion revealed a pronounced disproportional shift of ventilation and perfusion toward the nondependent lung. Overall, the dependent lung was minimally ventilated and perfused, but remained aerated with minimal detectable lung collapse. Perfusion was found primarily around the hilum of the nondependent lung and was minimal in the periphery of the nondependent and the entire dependent lung. These shifts can explain the high amount of venous admixture and physiological dead space found in this study. Breath holding redistributed ventilation toward dependent and ventral lung areas. The findings of this study reveal important pathophysiological insights into the changes in lung ventilation and perfusion during immobilization of white rhinoceroses. These novel insights might induce a search for better therapeutic options and is establishing EIT as a promising monitoring tool for large animals in the field.

NEW & NOTEWORTHY Electrical impedance tomography measurements of regional ventilation and perfusion applied to etorphine-immobilized white rhinoceroses in lateral recumbency revealed a pronounced disproportional shift of the measured ventilation and perfusion toward the nondependent lung. The dependent lung was minimally ventilated and perfused, but still aerated. Perfusion was found primarily around the hilum of the nondependent lung. These shifts can explain the gas exchange impairments found in this study. Breath holding can redistribute ventilation.

breathing pattern; dead space; distribution of ventilation; etorphine; pulmonary perfusion

INTRODUCTION

Over the last 10 years the number of rhinoceroses killed by poachers exceeded 9,000 animals, pushing the African rhinoceroses closer to extinction (25; see Ref. 44a for poaching statistics). Chemical immobilization is an essential intervention facilitating active conservational management of the vulnerable white rhinoceros (*Ceratotherium simum*). Potent opioids like etorphine are used routinely for chemical immobilization in wild animals, causing a narcotic state, which can be fully antagonized with a potent opioid receptor antagonist (naltrexone) to allow the animal to return into its habitat immediately after the procedure. Chemical immobilization has to be used in rhinoceroses for various reasons as this technique allows for animals to be restrained, loaded into transport crates, and translocated between different locations. This becomes necessary to maintain genetic flow between small and geographically isolated groups, to reintroduce rhinoceroses back into areas of their former distribution range, or relocate problematic individuals. A strategy being used in combating the recent rhinoceros poaching epidemic in southern Africa is to cut off the horns from at-risk individuals and, thereby, reduce their poaching value. Rhinoceros are chemically immobilized so that the horn can be removed. The increase in poaching events has also resulted in rhinoceroses that suffer bullet injuries but are not killed. These rhinoceroses are chemically immobilized for assessment and treatment of their resulting wounds. However, immobilization for these conservational efforts bears a high risk of mortality due to significant opioid-

Correspondence: (m.mosing@murdoch.edu.au).

induced pulmonary impairment, including severe hypoxemia. Pulmonary impairment in immobilized rhinoceroses has been well documented with moderate to severe hypoventilation in white and black rhinoceroses in lateral recumbency (10, 14, 15, 23, 31, 38). High degrees of venous admixture were measured suggesting large areas of lung atelectasis contributing to the observed hypoxemia (9). Opioid-induced muscle rigidity and twitching adds to the hypoxemia due to the increase in oxygen consumption (14). Although these are all causes for hypoxemia and hypercapnia, no conclusive reason for the poor gas exchange has been substantiated.

Electrical impedance tomography (EIT) is a noninvasive functional imaging modality used to evaluate distribution of pulmonary ventilation and perfusion (8, 12, 21, 22, 37, 43, 52). A belt with 32 equally-distanced mounted electrodes is placed around the thorax in a transverse plane. A small alternating current is applied between two electrodes, and the resulting voltages measured by the remaining electrodes are used to calculate electrical impedance. Then the pair of electrodes is deactivated, and the next pair around the belt is activated to calculate another set of impedance measurements (47). This process is repeated sequentially for all of the electrode pairs around the belt. Using software, these values are then used to reconstruct a transverse tomographic image of regional impedance values. The duty cycle of the rotation is much faster than the breathing rate so each individual cross-sectional image is effectively made under static circumstances. Depending on the EIT device, between 40 and 50 of such sequential images can be created each second. Sequential viewing of the images shows changes in regional distribution of impedance over time (54). The cyclic changes of gas within the alveoli and blood content within the vessels and the heart cause variations in impedance within the thorax (53). Perfusion-related impedance changes however are of a much smaller magnitude compared with ventilation-related changes. Highly concentrated saline (ionized sodium and chloride) conducts electrical current well; therefore, it can be used as an electrically conductive contrast agent to enhance the small changes in impedance caused by changing blood flow through the lungs. First-pass kinetics of a bolus of hypertonic saline can be used to create an EIT-indicator dilution curve and the corresponding contrast-enhanced lung perfusion images to determine the distribution of pulmonary perfusion (13).

The largest species on which EIT has been used, to date, is the horse (2, 3, 33, 34), but the EIT working principle of active electrodes does not limit its use to any size of animal as long as the electrode belt is long enough, the current sufficiently high and stable, and the distance between the actual electrodes and their preamplifiers not too long. Acquiring lung images in immobilized rhinoceroses might help in understanding the pathophysiology of impaired gas exchange and in finding strategies to mitigate adverse cardiorespiratory effects. EIT is the first imaging technique that might be applicable in these large mammals and be suitable for use under field conditions.

The aim of this study was to measure the distribution of ventilation and perfusion by EIT in rhinoceroses to understand the reason for the severe gas exchange impairments reported during immobilization. The findings should ultimately help in designing therapeutic interventions and new monitoring options which decrease complications and mortality in rhinoceroses during immobilization for conservational purposes.

METHODS

Ethical approval. This prospective, observational study was approved by the Institutional Animal Ethics committee of Murdoch University, Australia (permit number R2988/17) and the South African National Parks Animal Use and Care Committee (SANParks; reference number 001/16).

Animals. Six male subadult white rhinoceroses, weighing between 1,004 and 1,214 kg, were kept in holding facilities (bomas) in Kruger National Park, South Africa (238499609S, 318309909E; altitude 317 m) and managed according to SANParks Standard Operating Procedures for the Capture, Transportation and Maintenance in Holding Facilities of Wildlife. Animals had access to a mixture of lucerne and teff hay until the evening before the experiment, and to water ad libitum until the morning of the anesthesia. Food intake, defecation, and general demeanor were assessed daily.

Immobilization. The rhinoceroses were immobilized with a combination of etorphine hydrochloride (9.8 mg/mL, M99, Elanco, Gauteng, South Africa) and azaperone (40 mg/mL, Janssen Pharmaceutical, Halfway House, South Africa) plus hyaluronidase IM (5000 IU, Kyron Laboratories, Gauteng, South Africa). Drugs were administered into the nuchal hump by a 3.0-mL plastic dart with a 60-mm needle fired from a CO_2-powered dart-gun (DAN-INJECT International, Skukuza 1350, South Africa). Doses were selected on the basis of previously measured body mass (body weight of 1,000 to 1,250 kg: 2.5 mg etorphine, 37.5 mg azaperone, 5,000 IU hyaluronidase; body weight of 1,250 to 1,500 kg: 3.0 mg etorphine, 45 mg azaperone, 5,000 IU hyaluronidase). After darting, 5 of 6 rhinoceroses were in sternal recumbency when approached. One rhinoceros was in left lateral and was turned into sternal.

Instrumentation and monitoring set-up. For the EIT measurement a custom-made, 210-cm-long neoprene belt was built with 32 equidistantly mounted electrodes. Each electrode was underlaid by a 5 × 3 cm sponge, which was prefilled with nonconductive ultrasound gel before darting.

The immobilized rhinoceros was rolled from sternal to lateral recumbence onto a metal rail (100 cm length × 8 cm height × 10 cm width) with a broad central channel. The rail was positioned just caudal to the scapula and perpendicular to the spine. The EIT belt was pulled with a hook through the channel in the rail under the recumbent rhinoceros and fastened around the thorax 3–5 cm caudal to the elbow (6th–7th intercostal space) with reference electrode one placed at the left side of the sternum (46). The belt was closed and tightened to squeeze gel from the sponges underlying the electrodes to improve skin-electrode contact and then connected to the EIT device BBVet (SenTec, EIT branch, Landquart, Switzerland), which displayed and recorded the EIT data on a laptop computer at a rate of 48 frames per second.

Two modified equine endotracheal tubes (V Kruuse I.D. 28, CAT. No. 282270, Jørgen Kruuse A/S, Langeskov, Denmark) were inserted into each nostril and the cuffs inflated until airflow around the tubes ceased. The distal ends of both tubes were connected via a T-piece, which was connected to a capnograph and spirometer by a corrugated tube (PowerLab Exercise Physiology System ML870B80, ADInstruments, Bella Vista, NSW, Australia) to measure tidal volume (V_T) and end-tidal carbon dioxide ($P_{ET}CO_2$). Expired air was collected into a Douglas bag for 1 min at each sampling interval and analyzed for mixed-expired carbon dioxide partial pressure ($P\bar{E}T_{CO_2}$) using a second capnograph (Cardiocap/5, Datex-Ohmeda, GE Healthcare, Helsinki, Finland).

After aseptic skin preparation a 22-G catheter (Nipro Safelet Cath, Nipro, Bridgewater Township, NJ) was placed in the auricular artery and a 200-cm-long pulmonary artery catheter was inserted under ultrasound guidance into the linguofacial branch of the jugular vein and under observation of the pressure waveform, advanced into the pulmonary artery. The pressure transducers were zeroed and positioned at the height of the manubrium sterni and mean systemic (MAP) and pulmonary artery pressures (mPAP) were measured (Cardiocap/5 Datex-Ohmeda, GE Healthcare, Helsinki, Finland). Cardiac output ($\dot{Q}$) was

measured in triplicate by thermodilution (PM-9000 Vet veterinary portable multiparameter patient monitor, ShenZhen Mindray Bio-Medical Electronics, Nanshan, ShenZhen, China) using 60 mL of cold isotonic saline injected by hand in <3 s into the linguofacial vein catheter. Detailed description of the placement method for the pulmonary artery catheter and cardiac output measurements can be found elsewhere (10).

Heart rate (HR) and breathing frequency (F_b) were measured continuously by auscultation and observation of thoracic and abdominal excursions.

After finishing data collection, enrofloxacin 5 mg/kg (Baytril 100, Bayer, Isando, South Africa) and meloxicam 0.5 mg/kg (Metacam, Boehringer Ingelheim, Randburg, South African) were administered intramuscularly. At the end of data recording, all monitoring equipment including the EIT belt was disconnected and removed from the rhinoceros, naltrexone (Naltrexone, Kyron Laboratories, Benrose 2011, South Africa), 20 times the etorphine dose (mg), administered intramuscularly, and the animal observed until fully recovered.

Data collection. All monitoring variables (HR, F_b, $\dot{Q}$, MBP, mPAP, V_T, $P_{ET_{CO_2}}$) were recorded 30 (T30), 40 (T40), and 50 (T50) minutes after the animal was rolled to left lateral recumbency (Fig. 1). Two of the six rhinoceroses received an injection of butorphanol (10 mg for every 1 mg of etorphine; Wildlife Pharmaceuticals, White River 1240, South Africa) intravenously into an auricular vein after data collection at T30 as per anesthetic protocol of an unrelated study looking at drug interactions (9).

EIT data were recorded over 3 min at the three time points. Arterial and mixed-venous blood was sampled anaerobically from the auricular and pulmonary arteries for immediate analysis of arterial and mixed-venous oxygen (Pa_{O_2} and $P\bar{v}_{O_2}$) and carbon dioxide (Pa_{CO_2} and $P\bar{v}_{CO_2}$) partial pressures using a handheld blood gas analyzer (EPOC Blood Analysis System, Siemens Medical Solutions, Malvern, PA). Values were corrected to pulmonary artery temperature.

Ten minutes after finishing data collection at T50, a final EIT data recording was commenced during which 130 mL of 23% hypertonic saline was injected manually through the side port of the introducer in the linguofacial vein as rapidly as possible (10–15 s). EIT data recording was continued for another minute after the end of injection.

Barometric pressure was recorded from the blood gas analyzer.

Post hoc data analysis. A finite element (FE) thoracic model was constructed using information from photographs taken of an anatomically dissected rhinoceros specimen obtained from an animal killed by poachers (18–24 mo of age, male, ~600 kg) (Fig. 2*A*). Based on this FE model, the outer contour and the regions of interest (ROI) representing the right and left lung and the heart were defined (Fig. 2*B*). For EIT data analysis, a modified Graz consensus reconstruction algorithm for EIT (GREIT) (1) adapted to the rhinoceros's anatomy represented by the FE model was used to reconstruct EIT images for each animal delivering breathing-related (ΔZ_V) and perfusion-related (ΔZ_Q) regional changes of impedance (Fig. 2*C*). Further details on EIT technology and image reconstruction can be found elsewhere (1, 21, 49).

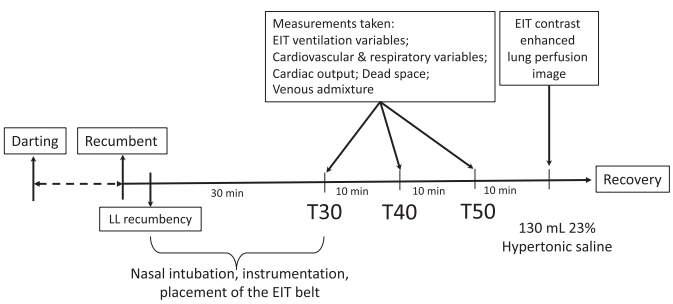

Fig. 1. Timeline of the study period and measurement time points 30 (T30), 40 (T40), and 50 (T50) minutes after the rhinoceros was rolled in left lateral (LL) recumbency and the injection of hypertonic saline after 60 min. The parameters measured at each time point are indicated in the boxes above the time line. EIT, electrical impedance tomography.

EIT data from between 6 to 15 consecutive breaths at each measurement point were analyzed to determine the impedance change for each pixel from start to end of inspiration using the dedicated software ibeX (SenTec, EIT branch, Landquart, Switzerland) (44). For the perfusion measurements based on contrast-enhanced lung perfusion imaging, the baseline impedance distribution was recorded before injecting the contrast agent (130 mL 23% hypertonic saline) into the linguofacial vein, and the EIT-indicator dilution curve was recorded (13). The maximal drop of global impedance over the time course of the curve was selected. The perfusion image was then calculated as the difference between the maximal drop of impedance and the reference values (Fig. 3).

Following EIT parameters were calculated for T30, T40 and T50:

1. The sum of the impedance changes within the predefined ROIs for the right (ΔZ_{V_R}) and the left (ΔZ_{V_L}) lung were evaluated. Based on this, the impedance ratio of right to left lung was calculated as $\Delta Z_{V_R}/\Delta Z_{V_L}$.
2. The center of ventilation right-to-left ($CoV_{R\text{-}L}$) and ventral-to-dorsal ($CoV_{V\text{-}D}$) were assessed. The CoV is a previously described parameter to express the geometric focal point of overall ventilation as a single digit in percent (32). The gravity-dependent vertical ($CoV_{R\text{-}L}$) and horizontal ($CoV_{V\text{-}D}$) position of the CoV is then expressed as a percentage of the extension of the identified lung region in the respective direction. For $CoV_{R\text{-}L}$, 0% refers to ventilation occurring in the most nondependent right lung region and 100% in the most dependent left part, while for $CoV_{V\text{-}D}$, 0% refers to ventilation occurring in the most ventral lung region of both lungs and 100% in the most dorsal part (Fig. 2*D*).
3. Nondependent and dependent silent spaces (NSS and DSS, respectively) were calculated as described previously (45, 48, 51). For a given breath, pixels within the previously defined two lung ROIs showing ventilation-induced ΔZ_V values of <10% of the maximum value were determined. A virtual line perpendicular to the gravity vector through the $CoV_{R\text{-}L}$ defined the ventilation horizon. All pixels lying below this ventilation horizon and showing ventilation-induced ΔZ_V values of <10% of the maximum value defined the DSS as percentage of all pixels within both lung ROIs. Accordingly, the NSS value describes the percentage of poorly ventilated pixels physically located above the ventilation horizon (48, 51) (Fig. 2*D*).
4. To describe the ventrodorsal distribution of ventilation during inspiration in more detail, the predefined lung ROIs were divided into four stacked regions of interest each covering 25% of the ventrodorsal horizontal distance of the right (R) and left (L) of lung (ventral 25% = ROI_{R_V} and ROI_{L_V}; central ventral 25% = $ROI_{R_{CV}}$ and $ROI_{L_{CV}}$; central dorsal 25% = $ROI_{R_{CD}}$ and $ROI_{L_{CD}}$; dorsal 25% = ROI_{R_D} and ROI_{L_D}) (39) (Fig. 2*E*).
5. The contrast-enhanced perfusion image at the time of the maximum drop in baseline impedance was compared visually to the respective ventilation image for match of pixels with maximal impedance change and areas of minimal perfusion and ventilation. The sum of the impedance changes of all pixels was evaluated as a percentage for ROI_{Q_R} and ROI_{Q_L} representing the percentage of the total pulmonary blood flow directed to the right and the left lung, respectively.

Venous admixture (Qs/Qt) at T30, T40, and T50 was calculated using Berggren's equation (7). In this equation, the percentage of arterial and mixed-venous hemoglobin saturated with O_2 was corrected using the table published by Reiners and colleagues (42).

Enghoff dead space was calculated using the standard equation (19):

$$VD_{Eng} = (Pa_{CO_2} - P\bar{E}T_{CO_2})/Pa_{CO_2}.$$

Very distinct breathing patterns were observed during the immobilization of the rhinoceroses, which included different levels of breath

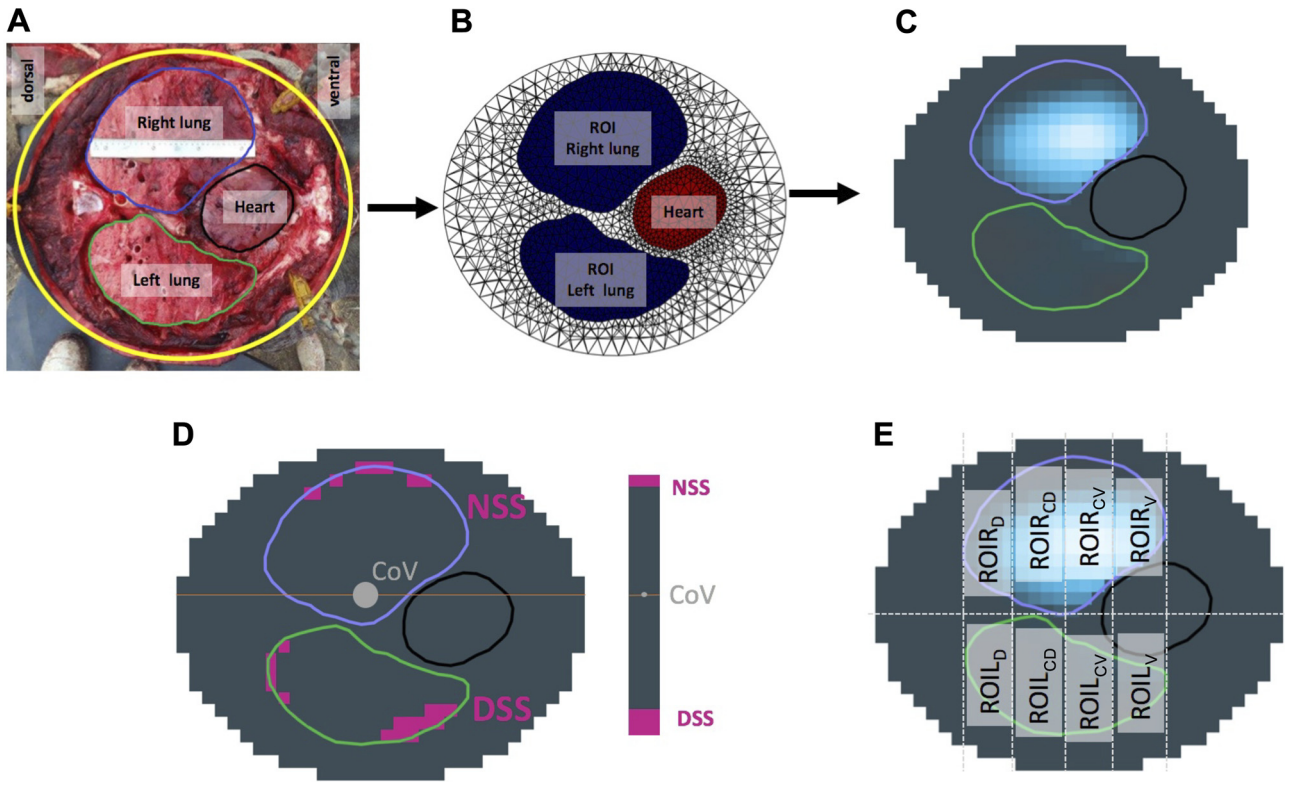

Fig. 2. Construction of a finite element model (*B*) using a transverse section of a rhinoceros specimen (*A*). EIT image showing ventilation-induced impedance changes (ΔZV) within the regions of interest (ROI) (*C*). From this image, the center of ventilation between the right and the left lung ($CoV_{R\text{-}L}$) and dependent (DSS) and nondependent (NSS) silent spaces were evaluated (*D*). The lung areas can be divided into four stacked regions of interest each covering 25% of the ventrodorsal height of the right (R) and left (L) lung (ventral 25% = $ROIR_V$ and $ROIL_V$; central ventral 25% = $ROIR_{CV}$ and $ROIL_{CV}$; central dorsal 25% = $ROIR_{CD}$ and $ROIL_{CD}$; dorsal 25% = $ROIR_D$ and $ROIL_D$) to describe distribution of ventilation (*E*).

holding. Categorization was created retrospectively to allow inclusion of this feature in our analysis and to avoid any unidentified confounding effects. Based on the impedance curve at each measurement point, the shape of the expiratory part was used to assign a breath holding category from A to E (BhC A–E): where category A was defined as linear-concave expiration curve with no signs of breath holding (BhC A), category B as irregular expiration curve with little signs of breath holding (BhC B), category C as "double-stroke breathing" with a deep

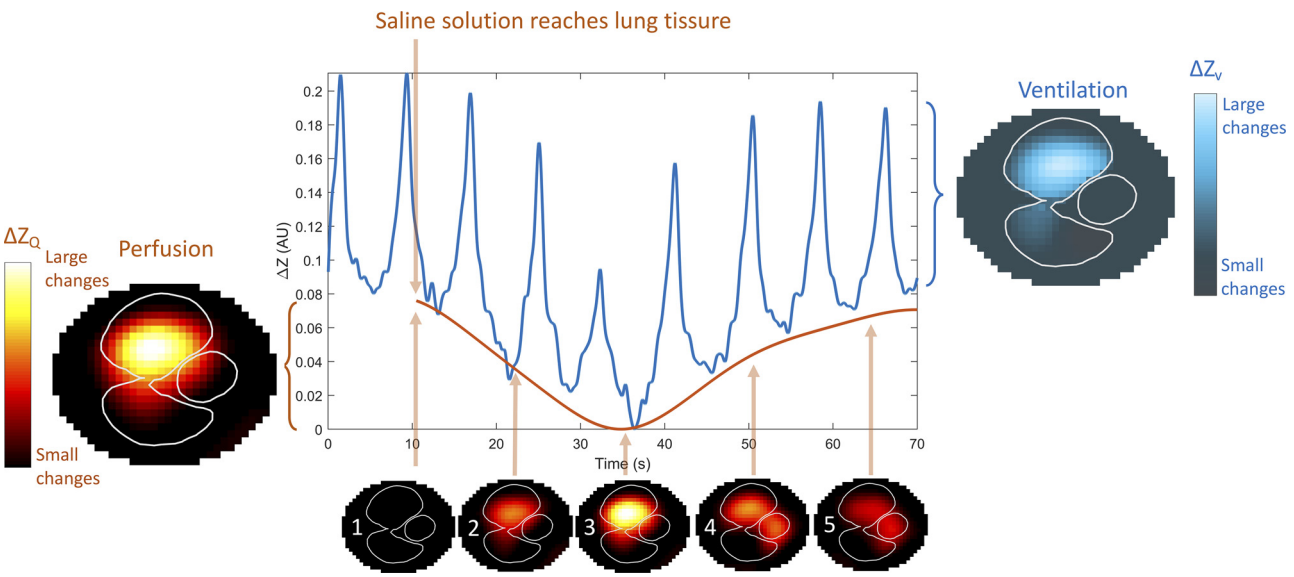

Fig. 3. Ventilation-induced impedance change curve in blue and the EIT-indicator dilution curve in red in a rhinoceros. One corresponding ventilation image and the contrast-enhanced perfusion image are illustrated on the right and left side of the curve, respectively. Lighter colors in the ventilation (ΔZv) and perfusion (ΔZ_Q) images correspond to higher changes in impedance from baseline. Perfusion images at different time points are shown below the dilution curve (*1*); before the indicator (23% hypertonic saline) is reaching the lung (*2*); graduate increase of the indicator in the nondependent lung (*3*); maximum (*4*, *5*) graduate decrease of indicator from the lung via the left heart.

breath followed by a small breath (BhC C), category D as biphasic expiration with distinct part of V_T (>50% drop in recorded impedance change) expired followed by breath holding (BhC D), and category E as inspiratory breath holding (BhC E) (Fig. 4). At least 80% of all analyzed breaths during one measurement period had to fall within one category to be classified as a specific BhC. If less than 80% of analyzed breaths fell within 1 of the 5 categories, this measurement was excluded from further evaluation of BhC.

Statistics. Results are given as means ± standard deviation (SD). The mean impedance change from all analyzed breaths was included in the statistical analysis.

The ΔZ_V was explored for an effect of region, side, and time using a mixed linear model accounting for the repeated measurements on each subject nested within BhC, using a covariance structure of compound symmetry. Selected post hoc pairwise comparisons were made against a Tukey's adjusted P value where there were significant interaction effects at $P \leq 0.05$.

Comparisons of summated ΔZ_V between left and right lungs were compared using a paired t-test with $P \leq 0.05$. The effect of BhC on $\Delta Z_{V_{R/L}}$ was evaluated for $CoV_{R\text{-}L}$ and $CoV_{V\text{-}D}$ using a general linear model with post hoc pairwise comparisons made to BhC A (no breath holding) against a Dunnett's corrected P value ≤ 0.05.

Multiple linear regression was used to explored the best subset explanation of variance in Qs/Qt and VD_{Eng}, including possible explanatory variables $\Delta Z_{V_{R/L}}$, $CoV_{R\text{-}L}$, $CoV_{V\text{-}D}$, $\dot{Q}$, mPAP, DSS, NSS. The simplest subset was selected based on the maximum adjusted R^2 and smallest Mallow's p (Cp).

RESULTS

All rhinoceroses recovered well after data collection for this study. Complete data sets from six rhinoceroses were included in the statistical analysis. Cardiac output measurements could not be obtained in two animals at one time point each due to technical issues. EIT-based regional perfusion was determined in two animals only.

Results for all recorded and calculated variables are given in Table 1 and for all EIT variables in Table 2. None of the measured and calculated EIT variables showed a significant change over time (T30-T50).

The nondependent right lung was preferentially ventilated in all rhinoceroses with a significantly higher ΔZ_{V_R} than ΔZ_{V_L} ($P < 0.0001$). Minimal NSS was detected by the EIT. Mean DSS over all measurements was below 6%. When reviewing all measurements, DSS represented an out-of-phase signal with respect to ventilation.

In the right lung, the central slices $ROI_{R_{CV}}$ and $ROI_{R_{CD}}$ showed a significantly higher ventilation (higher impedance) compared with the most ventral and dorsal slices ($P < 0.0001$). In the left lung, $ROI_{L_{CD}}$ showed a significantly higher impedance change than the other three ROIs which were only minimally ventilated ($P < 0.0001$).

At least 80% of all breaths during each measurement could be assigned to one breath holding category with a median of 100 (range: 84–100) % of the breath matching one specific BhC. Three of the six rhinoceroses changed their breathing pattern after T30 without any further changes. The breathing patterns of the other three rhinoceroses remained within one BhC throughout the study period. The breathing pattern had a significant effect on $\Delta Z_{V_{R/L}}$ ($P = 0.0011$) with breath holding after an initial partial expiration (BhC D; $P = 0.013$) resulted in a significantly lower $\Delta Z_{V_{R/L}}$ than no breath holding (BhC A); thus,

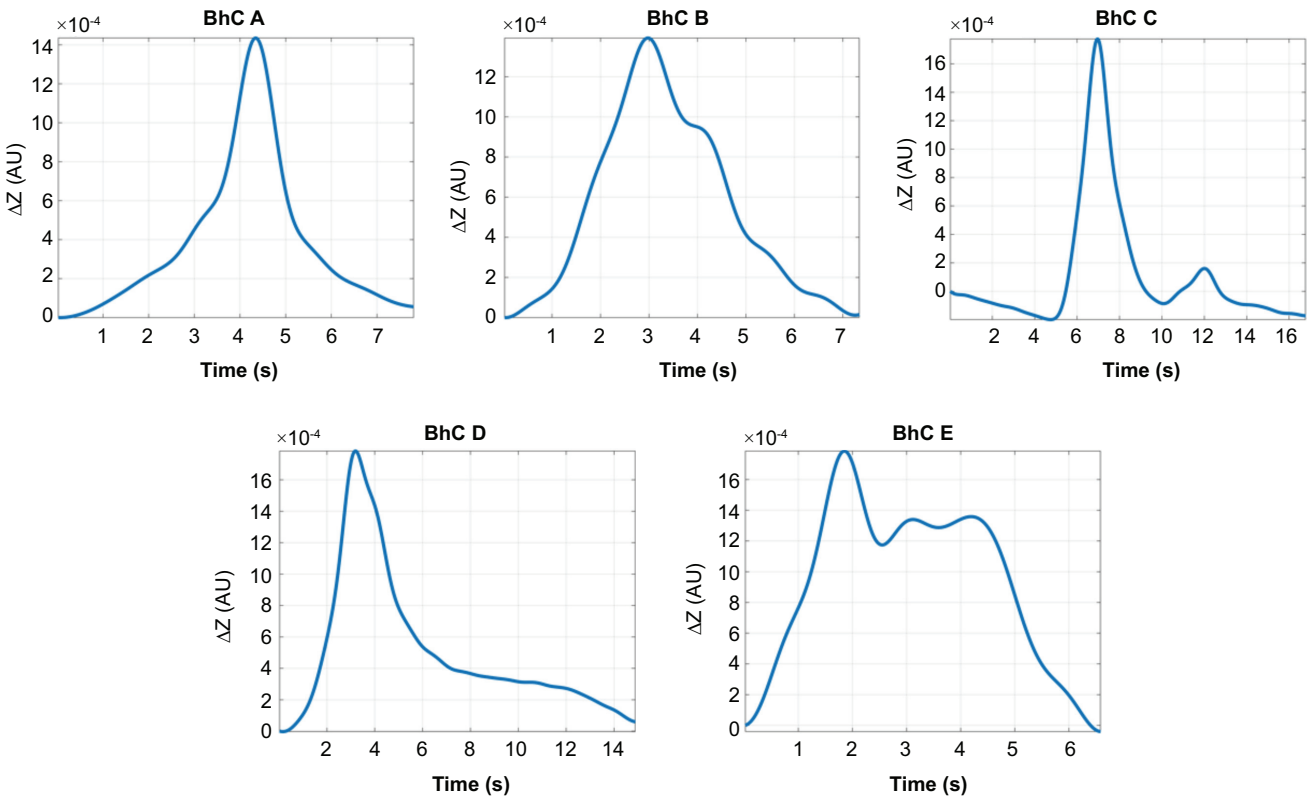

Fig. 4. Examples of impedance curves for each the breath holding categories (BhC): *1*: no signs of breath holding; *2*: irregular expiration curve with little signs of breath holding; *3*: "double-stroke breathing"; *4*: biphasic expiration; and *5*: inspiratory breath holding. ΔZ: impedance change in arbitrary units (AU), s: seconds.

Table 1. *Variables of recorded and calculated physiologic monitoring*

	Time Point in Left Lateral Recumbency		
	T30	T40	T50
Heart rate, beats/min	119 ± 17	93 ± 28	85 ± 25
Respiratory rate, breaths/min	7 ± 2	8 ± 2	8 ± 2
Cardiac output, L/min	9.1 ± 2.4	7.3 ± 2.7	6.5 ± 2.0
Mean blood pressure, mmHg	121.7 ± 20.8	96.5 ± 26.8	102.5 ± 29.4
Mean pulmonary pressure, mmHg	52.8 ± 3.7	46.0 ± 8.8	42.0 ± 9.7
$P_{ET_{CO_2}}$, mmHg	80.7 ± 9.0	70.3 ± 10.8	71.0 ± 6.7
Pa_{CO_2}, mmHg	88.6 ± 4.6	81.0 ± 13.0	82.2 ± 10.1
Pa_{O_2}, mmHg	28.9 ± 3.9	41.6 ± 16.7	40.3 ± 12.1
Venous admixture	0.53 ± 0.17	0.45 ± 0.22	0.47 ± 0.26
VD_{Eng}	0.56 ± 0.04	0.58 ± 0.04	0.61 ± 0.03
V_T, L	16.7 ± 5.0	12.8 ± 2.5	11.6 ± 2.9

Variables are presented over three time points in mean ± standard deviation. $P_{ET_{CO_2}}$, end-tidal carbon dioxide; Pa_{CO_2}, arterial carbon dioxide partial pressure; Pa_{O_2}, arterial oxygen partial pressure; VD_{Eng}, Enghoff's dead space; V_T, tidal volume

more of the dependent left lung was ventilated for BhC D compared with BhC A. The $\Delta Zv_{R/L}$ was not significantly different for BhC B, BhC C, and BhC E compared with BhC A.

A significant effect of BhC was also observed on $CoV_{R\text{-}L}$ ($P = 0.034$) and $CoV_{V\text{-}D}$ ($P = 0.002$). A shift of ventilation toward the dependent left lung was significantly related to the breathing pattern BhC D ($P = 0.050$) and toward the ventral parts to BhC E compared with BhC A.

Creation of perfusion images was possible in two rhinoceroses only (Fig. 5). In the other four rhinoceroses, the EIT-indicator dilution curve after injection of hypertonic saline could not be identified clearly in the EIT signal due to measurement artefacts and therefore the regional perfusion image could not be evaluated. One of these two rhinoceroses received butorphanol after T30 (rhino A), while the other did not (rhino B).

The two contrast-enhanced lung perfusion images showed a similar pattern (Fig. 5). When visually matching the ventilation image with the contrast enhanced lung perfusion images, the minimally ventilated dependent lung was also minimally perfused. The maximal perfusion was located around the hilum of the nondependent lung, which matched maximal ventilation in rhino A, but not in rhino B. No impedance change was found in the periphery of the nondependent lung in both the ventilation and perfusion images. However, these silent parts in the periphery of the nondependent lung were larger on perfusion images compared with the ventilation images in both rhinoceroses.

In the two rhinoceroses only 22% and 18% of the total blood flow was directed toward the dependent left ROI, respectively. The blood flow was mainly redirected to the nondependent lung with 78 and 82% of the total blood flow for rhino A and B, respectively.

All rhinoceroses showed systemic and pulmonary hypertension. The range for mPAP was 29 to 57 mmHg with a mean of 46.94 ± 8.69 mmHg over all measurements. Qs/Qt was high in all rhinoceroses with 0.48 ± 0.21 over all measurements. A decrease in mPAP and Qs/Qt was observed at T40 and T50 for the two rhinoceroses receiving butorphanol after data collection for T30. All rhinoceroses had VD_{Eng} values > 0.5 at any measurement point with a mean of 0.58 ± 0.04. None of the measured and calculated values or EIT variables explained any change in VD_{Eng}.

The variance in Qs/Qt was best described by the variance in $\dot{Q}$ ($R^2 = 0.61$). The next best single variable was mPAP ($R^2 = 0.13$), however, when $\dot{Q}$ and mPAP were combined in the model, the adjusted R^2 decreased by 0.04, suggesting that any effect of mPAP was already explained by $\dot{Q}$. None of the EIT variables had a relevant influence on Qs/Qt.

DISCUSSION

This study demonstrates that immobilized rhinoceroses in lateral recumbency preferentially ventilate the nondependent lung and that this distribution of ventilation is influenced by breath holding. The dependent lung remains aerated but is not ventilated and only minimally perfused. Lung perfusion was primarily detected around the hilum of the nondependent lung showing a distinct central-peripheral gradient with a lack of perfusion in lung periphery. Values for venous admixture were high as was Enghoff dead space. Changes in venous admixture were more influenced by changes in cardiac output and pulmonary pressure than by changes in the distribution of ventilation.

The main finding of the study, namely that more than 80% of ventilation occurred in the nondependent right lung, can be explained by the static compliance curve drawn by plotting transpulmonary pressure over lung volume (28) (Fig. 6).

Due to the loss in functional residual capacity during anesthesia and the mere size of the rhinoceros' lungs, the volume of the dependent lung drops causing a shift of this lung toward the flat noncompliant lower part of the compliance curve. Due to this loss of lung volume in the dependent lung, the nondependent lung, which normally contains large and noncompliant alveoli as represented by the shallow noncompliant upper part of the curve in the awake state, moves downward into the steep portion

Table 2. *Electrical impedance tomography variables*

	Time Point in Left Lateral Recumbency		
	T30	T40	T50
$CoV_{R\text{-}L}$, %	39.8 ± 3.6	39.6 ± 3.9	39.9 ± 4.2
$CoV_{V\text{-}D}$, %	52.0 ± 2.2	51.5 ± 1.9	51.0 ± 2.1
NSS, %	0.5 ± 1.1	1.0 ± 1.7	1.1 ± 1.9
DSS, %	5.1 ± 3.4	4.4 ± 2.4	4.2 ± 1.9
ΔZv_R, %	84.4 ± 7.8	84.6 ± 8.8	84.1 ± 9.1
ΔZv_L %	15.6 ± 7.8	15.4 ± 8.8	15.9 ± 9.1
$\Delta Zv_R/\Delta Zv_L$	6.5 ± 2.8	7.6 ± 4.9	6.9 ± 3.7
$ROIR_V$	11.8 ± 1.5	11.6 ± 1.9	12.2 ± 1.8
$ROIR_{CV}$	30.3 ± 3.3	30.7 ± 2.6	30.8 ± 2.9
$ROIR_{CD}$	31.0 ± 3.3	31.0 ± 4.5	30.3 ± 4.5
$ROIR_D$	11.2 ± 1.6	11.2 ± 2.1	10.7 ± 2.0
$ROIL_V$	0.3 ± 0.8	0.6 ± 0.9	0.5 ± 1.1
$ROIL_{CV}$	2.3 ± 2.4	3.0 ± 2.9	3.2 ± 3.1
$ROIL_{CD}$	9.3 ± 5.2	8.8 ± 5.2	9.0 ± 5.6
$ROIL_D$	3.7 ± 2.2	3.0 ± 2.0	3.1 ± 1.8
BhC	3.2 ± 1.2	3.2 ± 1.5	3. ± 1.5

Variables are presented over three time points in mean ± standard deviation. $CoV_{R\text{-}L}$, center of ventilation right-to-left; $CoV_{V\text{-}D}$, center of ventilation ventral-to-dorsal; NSS, nondependent silent space; DSS, dependent silent space; ΔZv_R, impedance change within the right lung; ΔZv_L, impedance change within the left lung; $\Delta Zv_R/\Delta Zv_L$, impedance ratio of right to left lung; $ROIR_V$, region of interest right lung ventral; $ROIR_{CV}$, region of interest right lung central ventral; $ROIR_{CD}$, region of interest right lung central dorsal; $ROIR_D$, region of interest right lung dorsal; $ROIL_V$, region of interest left lung ventral; $ROIL_{CV}$, region of interest left lung central ventral; $ROIL_{CD}$, region of interest left lung central dorsal; $ROIL_D$, region of interest left lung dorsal; BhC, breath holding category.

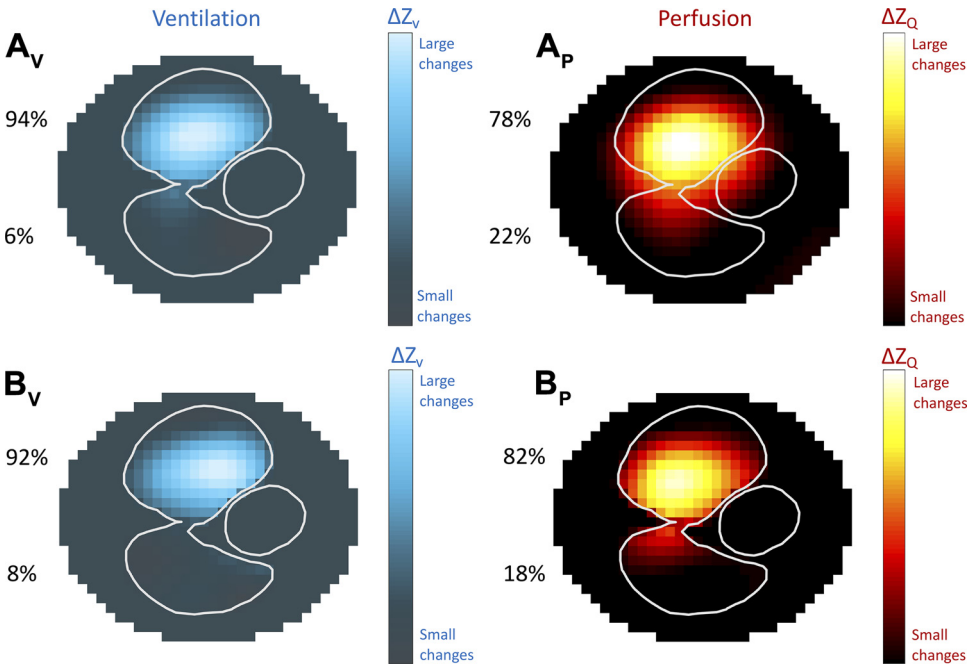

Fig. 5. Ventilation (A_V and B_V) and contrast enhanced lung perfusion (A_P and B_P) images of rhino A and rhino B. The sum of the ventilation induced (ΔZ_V) and perfusion induced (ΔZ_Q) impedance changes within the predefined regions of interests (ROI) for the right and the left lung are given in percentage of the total impedance change in both ROIs.

of the compliance curve and therefore becomes preferentially ventilated (40, 41). A distinct preference of ventilation of the nondependent lung, as in our rhinoceroses, has also been found in anesthetized ponies under controlled mechanical ventilation in right lateral recumbency (4). The shift of ventilation toward the nondependent lung observed in rhinoceroses and horses might be explained by the fact that both belong to the taxonomic order of *Perissodactyla* and have a very similar gastrointestinal tract (27). In these animals the diaphragmatic flexure of the dorsal large colon makes considerable contact with the diaphragm and lies within the intrathoracic part of the abdominal cavity in standing *Perissodactyla* (27). In lateral recumbency it might impede movement of the dependent diaphragm and thus restrict lung expansion. The obstructive effect might impair the ventilation in the dependent lung as seen in our rhinoceroses.

The breath holding seen in 50% of the rhinoceroses might be the same peripheral chemoreceptor response to CO_2 as observed in woodchucks where laryngeal and diaphragmatic breaking was observed with increasing levels of inspiratory CO_2 up to 5% (11). An effort of autorecruitment with inspiratory breath holding was also observed in standing horses after anesthesia and was associated with increased Pa_{CO_2} levels (34) and in pigs after induced mild acute respiratory distress syndrome (35). In humans this reflex has been observed in preterm infants (17) and in COPD patients where it was discussed as an effort to create intrinsic PEEP (6). However, this phenomenon does not appear in other species like dogs, cats, or coatimundis as they activate the posterior cricoarytenoid muscles during expiration to keep upper airways open and reduce resistance to expiratory flow (5, 11, 20). The chemosensitivity to CO_2 in a species has been shown to be the main factor determining whether breath holding occurs, with less sensitive species showing this phenomenon to a greater extent (11). Our results, and the findings in horses, indicate that *Perissodactyla* possibly fall within the group of less sensitive species. Based on our findings this reflex might be a natural way to distribute inspired gas into less ventilated parts of the lungs.

Only minimal DSS were observed in all rhinoceroses over the entire study period suggesting minimal lung collapse of the dependent lung leaving the dependent lung aerated but not ventilated. The resulting low regional partial pressure of oxygen in the dependent lung caused hypoxic pulmonary vasoconstriction (HPV) resulting in a redistribution of blood toward the ventilated areas of the lung (29). The DSS observed in our study could be due to the weight of the heart compressing lung tissue or to a gas filled gastrointestinal viscus that moved into the EIT

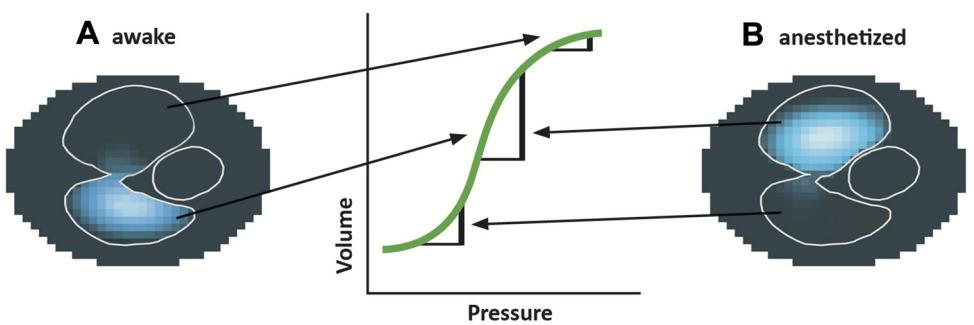

Fig. 6. Schematic diagram showing the static compliance curve (pressure-volume curve;) in an awake (*A*; hypothetical EIT image) and anesthetized (*B*; EIT image from a measurement) rhinoceros in lateral recumbency. During anesthesia the dependent lung units move from the steep, compliant part of the pressure-volume curve to the lower flat part of the curve, while the nondependent lung units move from the flat noncompliant into the steep compliant parts and therefore receive more ventilation during inspiration as seen on the electrical impedance tomography (EIT) image of an anesthetized rhinoceros in lateral recumbency.

plane during expiration. The same phenomenon was observed in standing horses (3) and very likely represented the impedance change caused by the breath-synchronous movement of aforementioned flexura diaphragmatica dorsalis of the large colon.

It is important to appreciate that Pa_{O_2} values in standing awake rhinoceroses are not different from values observed in other mammals, while slightly higher resting values for Pa_{CO_2} of 44 to 53 mmHg have been observed (16). In this study we could confirm the findings of earlier reports of severe hypoventilation, hypoxemia, and a substantial degree of venous admixture in our group of etorphine immobilized rhinoceroses compared with these values measured in unrestrained standing animals (10, 14–16). For the calculation of venous admixture, we used the values recently published for white rhinoceroses for the oxygen saturation of hemoglobin rather than those measured by the blood gas analyzer (42). This reduced venous admixture values markedly, but still left us with a percentage of venous admixture $> 45\%$ of cardiac output. We assume that the nonventilated dependent lung contributed to these high values, despite the HPV evidently observed on the perfusion images. This redistribution forces the cardiac output to flow through a diminished vascular bed causing an increase in blood flow and pulmonary pressure in these areas (29). The increase in pressure might be additionally enhanced by etorphine which has been shown to cause both systemic and pulmonary vasoconstriction (15, 30). High blood flow through a small proportion of the lung and high pressure are known to recruit intrapulmonary arteriovenous anastomoses in exercising horses and humans (18, 26). We were able to confirm these theories by our results showing that the magnitude of venous admixture was significantly influenced by cardiac output, while the influence of pulmonary pressure was directly linked to the influence of cardiac output on venous admixture. Statistically we were unable to show an influence of the distribution of ventilation on venous admixture. However, when visually matching the ventilation and perfusion image of the two rhinoceroses, rhino A, where maximal ventilation matched maximal perfusion, showed a Qs/Qt of 0.16 at T40, while rhino B, where the center of ventilation was not located close to the hilum of the nondependent lung, a Qs/Qt of 0.46 was observed. This suggests that simply looking at the match between the distribution of ventilation and Qs/Qt as a global factor for ventilation perfusion mismatch might be less sensitive then obtaining matched ventilation and perfusion images by EIT. Several studies have attempted to use EIT as a noninvasive monitoring method to evaluate ventilation-perfusion match, but no standard method is available yet (8, 12, 13, 37).

High Enghoff dead space values in black rhinoceroses in lateral recumbency have been reported previously (38). Based on our data, these values can be explained in two ways: first, the high venous admixture causes pulmonary artery blood, with its high $P\bar{v}_{CO_2}$, to bypass the lungs and increase Pa_{CO_2}, which is used in the Enghoff equation as a surrogate for alveolar CO_2. This disproportional increase in Pa_{CO_2} leads to an overestimation of real dead space (32, 50). Second, the primary vasoconstriction caused by etorphine (30), plus the fact that pulmonary perfusion pressure decreased by 1 cmH_2O for each centimeter of elevation that blood flow has to travel above heart level (28), resulted in peripheral regions of the nondependent well-ventilated lung not receiving any blood flow as observed in our perfusion images (Fig. 5). The ventilated gas volume lacking contact with blood flowing through these lung units per definition constitutes real alveolar dead space and thus "wasted" ventilation as it does not contribute to gas exchange.

Based on our observations, the pathophysiological changes in lung function and $\dot{V}/\dot{Q}$ matching in particular of immobilized rhinoceroses can be better understood. These novel insights are hoped to contribute to safer immobilization protocols and procedures. One potential attempt to improve $\dot{V}/\dot{Q}$ matching could be to provoke vasodilation in the nondependent ventilated areas while at the same time maintaining HPV in the dependent lung. A drug that would fulfil these criteria is salbutamol, which has, as a beta 2 agonist, vasodilative effects and has been shown to enhance HPV (36). Salbutamol is also inexpensive, which is a necessary requirement in the light of the enormous size of the animals. Another potentially important learning from our study is the fact that increasing inspiratory oxygen concentrations may cause an increase in absorption atelectasis in the dependent lung which in our cohort of rhinoceroses seems to remain aerated under room air breathing and might therefore worsen return to normal ventilation after recovery (24). Indeed, oxygen supplementation has failed to show any significant effect on oxygenation in etorphine-immobilized rhinoceroses (23). Further studies evaluating lung collapse after oxygen supplementation are needed to confirm our assumption.

Furthermore, this study shows that breath holding might be an important compensatory mechanism to redistribute gas within the lungs. Future studies will have to evaluate whether the observed breath holding is due to laryngeal or diaphragmatic braking (11). In case laryngeal braking is contributing to this phenomenon, endotracheal intubation might impair this compensatory reflex in immobilized rhinoceroses.

One aim of our study was to evaluate the use of EIT under field conditions. We were able to obtain representative measurements with a commercially available device and a self-made belt. The EIT system used still required an external power supply, which was accessible in the boma situation in this study, but could easily be replaced by adequate batteries. The method for belt placement was quick and safe for both the animal and personnel involved. However, we were facing several challenges during the EIT data analysis of this study; first, to obtain spatially and functionally meaningful EIT images we had to first create a finite element (FE) model for rhinoceroses. FE models are generated to analyze EIT raw data in a correct anatomical shape, normally based on computed tomography (CT) imaging, which was not possible in rhinoceroses. Therefore, an FE model was created from photographs taken from a rhino during a postmortem investigation. An overhead hoist was used to hang the rhino to preserve as much as possible the correct anatomic structure. The body was cut with a bone saw at the assumed belt position to be used in the living animals. Based on the dimensions acquired from the images, the electrodes were placed equidistantly to create the contour and electrode planes for the lung, heart, and thorax. This allowed us to create two lung regions of interest and especially exclude most signals from the partially gas-filled dorsal colon moving into the EIT plane in the dependent parts during expiration. Second, guaranteeing good signal quality throughout the study period was difficult. The noise increased over time of the measurement period possibly due to desiccation of the gel in the sponges. Refilling the sponges with gel on the left side was not possible as we could not move the

animals into sternal during the measurements. However, washing the skin with water and decreasing the surface debris before putting on the belt might have allowed longer undisturbed measurement periods. In general, the EIT signal quality was adequate despite application of the contact gel to sponges located under the electrodes instead of applying the gel to the skin of the patient directly. This approach of preparing electrodes with gel before the actual measurement should allow EIT measurements in large animals also under field conditions.

We retrospectively set up a breath holding categorization based on the distinct breathing patterns we observed during data collection. A significant effect was found for the two breathing patterns showing breath holding. However, our categorization has never been validated and was simply based on observations. Therefore, the fact that no significant effect was found for minimal breath holding or double-stroke breathing is not conclusive. Future studies should investigate in more detail the impact of breath holding to elucidate the clinical relevance of different breathing patterns in a larger cohort of animals. Furthermore, the redistribution of ventilation into the open aerated dependent lung should be evaluated after position change. Based on current knowledge sternal (prone) recumbency might improve equilibration of ventilation between the two lungs compared with lateral in immobilized rhinoceroses, as the latter impairs gas exchange to a greater extent (31, 38).

Conclusions

The shift of ventilation and perfusion toward the nondependent lung may explain the severe impairment of gas exchange observed in immobilized white rhinoceroses. The dependent lung remained aerated but was not ventilated and only minimally perfused. Rhinoceroses appear to influence their distribution of ventilation by breath holding. Possible treatment options and clinical assumptions for future immobilizations based on these findings will need to be confirmed in future studies.

GRANTS

We thank the Stiftung Temperatio (Switzerland) and the Wiederhold Foundation (Torrington, Connecticut) for their financial support for this study.

DISCLOSURES

No conflicts of interest, financial or otherwise, are declared by the authors.

AUTHOR CONTRIBUTIONS

M.M., L.C.M., S.H.B., M.S., P.B., J.M.B., R.D.G. and M.M. conceived and designed research; M.M., L.C.M., M.S., P.B., J.M.B., G.E.Z., R.D.G. and M.M. performed experiments; M.M., S.H.B., A.D.W., M.S., J.M.B. and G.H. analyzed data; M.M., L.C.M., S.H.B., A.D.W., M.S., P.B., G.E.Z., G.H., and R.D.G. interpreted results of experiments; M.M. and A.D.W. prepared figures; M.M., S.H.B., A.D.W. and G.H. drafted manuscript; M.M., L.C.M., S.H.B., A.D.W., M.S., P.B., J.M.B., G.E.Z., G.H., R.D.G. and M.M. edited and revised manuscript; M.M., L.C.M., S.H.B., A.D.W., M.S., P.B., J.M.B., G.E.Z., G.H., R.D.G. and M.M. approved final version of manuscript.

REFERENCES

1. **Adler A**, **Arnold JH**, **Bayford R**, **Borsic A**, **Brown B**, **Dixon P**, **Faes TJ**, **Frerichs I**, **Gagnon H**, **Gärber Y**, **Grychtol B**, **Hahn G**, **Lionheart WR**, **Malik A**, **Patterson RP**, **Stocks J**, **Tizzard A**, **Weiler N**, **Wolf GK.** GREIT: a unified approach to 2D linear EIT reconstruction of lung images. *Physiol Meas* 30: S35–S55, 2009. doi:10.1088/0967-3334/30/6/S03.
2. **Ambrisko TD**, **Schramel J**, **Hopster K**, **Kästner S**, **Moens Y.** Assessment of distribution of ventilation and regional lung compliance by electrical impedance tomography in anaesthetized horses undergoing alveolar recruitment manoeuvres. *Vet Anaesth Analg* 44: 264–272, 2017. doi:10.1016/j.vaa.2016.03.001.
3. **Ambrisko TD**, **Schramel JP**, **Adler A**, **Kutasi O**, **Makra Z**, **Moens YP.** Assessment of distribution of ventilation by electrical impedance tomography in standing horses. *Physiol Meas* 37: 175–186, 2016. doi:10.1088/0967-3334/37/2/175.
4. **Auer U**, **Schramel JP**, **Moens YP**, **Mosing M**, **Braun C.** Monitoring changes in distribution of pulmonary ventilation by functional electrical impedance tomography in anaesthetized ponies. *Vet Anaesth Analg* 46: 200–208, 2019. doi:10.1016/j.vaa.2018.09.048.
5. **Bartlett D Jr.** Effects of hypercapnia and hypoxia on laryngeal resistance to airflow. *Respir Physiol* 37: 293–302, 1979. doi:10.1016/0034-5687(79)90076-8.
6. **Baz M**, **Haji GS**, **Menzies-Gow A**, **Tanner RJ**, **Hopkinson NS**, **Polkey MI**, **Hull JH.** Dynamic laryngeal narrowing during exercise: a mechanism for generating intrinsic PEEP in COPD? *Thorax* 70: 251–257, 2015. doi:10.1136/thoraxjnl-2014-205940.
7. **Berggren SM.** The oxygen deficit of arterial blood caused by non-ventilated parts of the lung. *Acta Physiol Scand* 4: 4–9, 1942.
8. **Bluth T**, **Kiss T**, **Kircher M**, **Braune A**, **Bozsak C**, **Huhle R**, **Scharffenberg M**, **Herzog M**, **Roegner J**, **Herzog P**, **Vivona L**, **Millone M**, **Dössel O**, **Andreeff M**, **Koch T**, **Kotzerke J**, **Stender B**, **Gama de Abreu M.** Measurement of relative lung perfusion with electrical impedance and positron emission tomography: an experimental comparative study in pigs. *Br J Anaesth* 123: 246–254, 2019. doi:10.1016/j.bja.2019.04.056.
9. **Boesch J.** *Respiratory, Cardiovascular and Metabolic Effects Of Etorphine, With And Without Butorphanol, in White Rhinoceros (Ceratotherium Simum)* (PhD Dissertation). Pretoria, South Africa: Univ. of Pretoria, 2019, p. 244.
10. **Boesch JM**, **Gleed RD**, **Buss P**, **Hofmeyr M**, **Tordiffe A**, **Zeiler G**, **Meyer L.** Effects of a supplemental etorphine dose on pulmonary artery pressure and cardiac output in immobilized, boma-habituated white rhinoceros (*Ceratotherium simum*): A preliminary study. *J Zoo Wildl Med* 49: 849–855, 2018. doi:10.1638/2017-0120.1.
11. **Boggs DF**, **Colby C**, **Williams BR Jr**, **Kilgore DL Jr.** Chemosensitivity and breathing pattern regulation of the coatimundi and woodchuck. *Respir Physiol* 89: 157–167, 1992. doi:10.1016/0034-5687(92)90047-Z.
12. **Borges JB**, **Cronin JN**, **Crockett DC**, **Hedenstierna G**, **Larsson A**, **Formenti F.** Real-time effects of PEEP and tidal volume on regional ventilation and perfusion in experimental lung injury. *Intensive Care Med Exp* 8: 10, 2020. doi:10.1186/s40635-020-0298-2.
13. **Borges JB**, **Suarez-Sipmann F**, **Bohm SH**, **Tusman G**, **Melo A**, **Maripuu E**, **Sandström M**, **Park M**, **Costa EL**, **Hedenstierna G**, **Amato M.** Regional lung perfusion estimated by electrical impedance tomography in a piglet model of lung collapse. *J Appl Physiol (1985)* 112: 225–236, 2012. doi:10.1152/japplphysiol.01090.2010.
14. **Buss P**, **Miller M**, **Fuller A**, **Haw A**, **Stout E**, **Olea-Popelka F**, **Meyer L.** Postinduction butorphanol administration alters oxygen consumption to improve blood gases in etorphine-immobilized white rhinoceros. *Vet Anaesth Analg* 45: 57–67, 2018. doi:10.1016/j.vaa.2017.03.008.
15. **Buss P**, **Miller M**, **Fuller A**, **Haw A**, **Wanty R**, **Olea-Popelka F**, **Meyer L.** Cardiovascular effects of etorphine, azaperone, and butorphanol combinations in chemically immobilized captive white rhinoceros (*Ceratotherium simum*). *J Zoo Wildl Med* 47: 834–843, 2016. doi:10.1638/2015-0298.1.
16. **Citino SB**, **Bush M.** Reference cardiopulmonary physiologic parameters for standing, unrestrained white rhinoceroses (*Ceratotherium simum*). *J Zoo Wildl Med* 38: 375–379, 2007. doi:10.1638/2006-0007R1.1.
17. **Eichenwald EC**, **Ungarelli RA**, **Stark AR.** Hypercapnia increases expiratory braking in preterm infants. *J Appl Physiol (1985)* 75: 2665–2670, 1993. doi:10.1152/jappl.1993.75.6.2665.
18. **Elliott JE**, **Duke JW**, **Hawn JA**, **Halliwill JR**, **Lovering AT.** Increased cardiac output, not pulmonary artery systolic pressure, increases intrapulmonary shunt in healthy humans breathing room air and 40% O2. *J Physiol* 592: 4537–4553, 2014. doi:10.1113/jphysiol.2014.274829.
19. **Enghoff H.** Volumen inefficax. Bemerkungen zur Frage des schädlichen Raumes. *Uppsala Lak Forhandl* 44: 191–218, 1938.
20. **England SJ**, **Harding R**, **Stradling JR**, **Phillipson EA.** Laryngeal muscle activities during progressive hypercapnia and hypoxia in awake and sleeping dogs. *Respir Physiol* 66: 327–339, 1986. doi:10.1016/0034-5687(86)90084-8.

21. **Frerichs I**, **Amato MB**, **van Kaam AH**, **Tingay DG**, **Zhao Z**, **Grychtol B**, **Bodenstein M**, **Gagnon H**, **Böhm SH**, **Teschner E**, **Stenqvist O**, **Mauri T**, **Torsani V**, **Camporota L**, **Schibler A**, **Wolf GK**, **Gommers D**, **Leonhardt S**, **Adler A**; **TREND study group.** Chest electrical impedance tomography examination, data analysis, terminology, clinical use and recommendations: consensus statement of the TRanslational EIT developmeNt stuDy group. *Thorax* 72: 83–93, 2017. doi:10.1136/thoraxjnl-2016-208357.
22. **Frerichs I**, **Hinz J**, **Herrmann P**, **Weisser G**, **Hahn G**, **Dudykevych T**, **Quintel M**, **Hellige G.** Detection of local lung air content by electrical impedance tomography compared with electron beam CT. *J Appl Physiol (1985)* 93: 660–666, 2002. doi:10.1152/japplphysiol.00081.2002.
23. **Haw A**, **Hofmeyr M**, **Fuller A**, **Buss P**, **Miller M**, **Fleming G**, **Meyer L.** Butorphanol with oxygen insufflation corrects etorphine-induced hypoxaemia in chemically immobilized white rhinoceros (*Ceratotherium simum*). *BMC Vet Res* 10: 253, 2014. doi:10.1186/s12917-014-0253-0.
24. **Hedenstierna G**, **Edmark L.** Mechanisms of atelectasis in the perioperative period. *Best Pract Res Clin Anaesthesiol* 24: 157–169, 2010. doi:10.1016/j.bpa.2009.12.002.
25. **Knight M.** African Rhino Specialist Group report. *Pachyderm* 59: 14–26, 2017.
26. **La Gerche A**, **Daffy JR**, **Mooney DJ**, **Forbes G**, **Davie AJ.** Transit of micro-bubbles through the pulmonary circulation of Thoroughbred horses during exercise. *Res Vet Sci* 95: 644–647, 2013. doi:10.1016/j.rvsc.2013.04.002.
27. **Langer P.** Perissodactyla. In: *Handbook of Zoology: Comparative anatomy of the Gastrointestinal Tract in Eutheria* , edited by Zachos FE**.** Berlin: Walter de Gruyter KG, 2017, p. 378–409.
28. **Lohser J**, **Ishikawa S.** Physiology of the lateral decubitus position, open chest and one-lung ventilation. In: *Principles and Practice of Anesthesia for Thoracic Surgery*, edited by Slinger P**.** New York: Springer, 2011, p. 71–82.
29. **Lumb AB**, **Slinger P.** Hypoxic pulmonary vasoconstriction: physiology and anesthetic implications. *Anesthesiology* 122: 932–946, 2015. doi:10.1097/ALN.0000000000000569.
30. **Meyer LC**, **Hetem RS**, **Mitchell D**, **Fuller A.** Hypoxia following etorphine administration in goats (Capra hircus) results more from pulmonary hypertension than from hypoventilation. *BMC Vet Res* 11: 18, 2015. doi:10.1186/s12917-015-0337-5.
31. **Morkel PV**, **Radcliffe RW**, **Jago M**, **du Preez P**, **Flaminio MJ**, **Nydam DV**, **Taft A**, **Lain D**, **Miller MM**, **Gleed RD.** Acid-base balance and ventilation during sternal and lateral recumbency in field immobilized black rhinoceros (*Diceros bicornis*) receiving oxygen insufflation: a preliminary report. *J Wildl Dis* 46: 236–245, 2010. doi:10.7589/0090-3558-46.1.236.
32. **Mosing M**, **Böhm SH**, **Rasis A**, **Hoosgood G**, **Auer U**, **Tusman G**, **Bettschart-Wolfensberger R**, **Schramel JP.** Physiologic factors influencing the arterial-to-end-tidal co_2 difference and the alveolar dead space fraction in spontaneously breathing anesthetised horses. *Front Vet Sci* 5: 58, 2018. doi:10.3389/fvets.2018.00058.
33. **Mosing M**, **Marly-Voquer C**, **MacFarlane P**, **Bardell D**, **Bohm SH**, **Bettschart-Wolfensberger R**, **Waldmann AD.** Regional distribution of ventilation in horses in dorsal recumbency during spontaneous and mechanical ventilation assessed by electrical impedance tomography: a case series. *Vet Anaesth Analg* 44: 127–132, 2017.
34. **Mosing M**, **Waldmann AD**, **MacFarlane P**, **Iff S**, **Auer U**, **Bohm SH**, **Bettschart-Wolfensberger R**, **Bardell D.** Horses auto-recruit their lungs by inspiratory breath holding following recovery from general anaesthesia. *PLoS One* 11: e0158080, 2016. doi:10.1371/journal.pone.0158080.
35. **Pellegrini M**, **Hedenstierna G**, **Roneus A**, **Segelsjö M**, **Larsson A**, **Perchiazzi G.** The diaphragm acts as a brake during expiration to prevent lung collapse. *Am J Respir Crit Care Med* 195: 1608–1616, 2017. doi:10.1164/rccm.201605-0992OC.
36. **Pillet O**, **Manier G**, **Castaing Y.** Anticholinergic versus beta 2-agonist on gas exchange in COPD: a comparative study in 15 patients. *Monaldi Arch Chest Dis* 53: 3–8, 1998.
37. **Putensen C**, **Hentze B**, **Muenster S**, **Muders T.** Electrical impedance tomography for cardio-pulmonary monitoring. *J Clin Med* 8: 1176, 2019. doi:10.3390/jcm8081176.
38. **Radcliffe RW**, **Morkel P**, **Jago M**, **Taft AA**, **du Preez P**, **Miller MA**, **Candra D**, **Nydam DV**, **Barry JS**, **Gleed RD.** Pulmonary dead space in free-ranging immobilized black rhinoceroses (*Diceros bicornis*) in Namibia. *J Zoo Wildl Med* 45: 263–271, 2014. doi:10.1638/1042-7260-45.2.263.
39. **Radke OC**, **Schneider T**, **Heller AR**, **Koch T.** Spontaneous breathing during general anesthesia prevents the ventral redistribution of ventilation as detected by electrical impedance tomography: a randomized trial. *Anesthesiology* 116: 1227–1234, 2012. doi:10.1097/ALN.0b013e318256ee08.
40. **Rehder K**, **Hatch DJ**, **Sessler AD**, **Fowler WS.** The function of each lung of anesthetized and paralyzed man during mechanical ventilation. *Anesthesiology* 37: 16–26, 1972. doi:10.1097/00000542-197207000-00004.
41. **Rehder K**, **Wenthe FM**, **Sessler AD.** Function of each lung during mechanical ventilation with ZEEP and with PEEP in man anesthetized with thiopental-meperidine. *Anesthesiology* 39: 597–605, 1973. doi:10.1097/00000542-197312000-00007.
42. **Reiners JK**, **Hellmann N**, **Schmidt J**, **Kästner SBR.** Odd haemoglobins in odd-toed ungulates: Impact of selected haemoglobin characteristics of the white rhinoceros (*Ceratotherium simum*) on the monitoring of the arterial oxygen saturation of haemoglobin. *PLoS One* 14: e0226851, 2019. doi:10.1371/journal.pone.0226851.
43. **Riedel T**, **Fraser JF**, **Dunster K**, **Fitzgibbon J**, **Schibler A.** Effect of smoke inhalation on viscoelastic properties and ventilation distribution in sheep. *J Appl Physiol (1985)* 101: 763–770, 2006. doi:10.1152/japplphysiol.01635.2005.
44. **Róka PL**, **Waldmann AD**, **Böhm SH**, **Karagiannidis C**, **Ender F.** Software tool for analysing ventilation EIT data. In: Proceedings of the 16th International Conference on Biomedical Applications of Electrical Impedance Tomography, edited by Sola J, Braun F, Adler A**.** Neuchatel, Switzerland: CSEM, 2016, p. 59.

44a. **Save the Rhino International.** Poaching Statistics. https://www.savetherhino.org/rhino-info/poaching-stats/

45. **Shono A**, **Katayama N**, **Fujihara T**, **Böhm SH**, **Waldmann AD**, **Ugata K**, **Nikai T**, **Saito Y.** Positive end-expiratory pressure and distribution of ventilation in pneumoperitoneum combined with steep trendelenburg position. *Anesthesiology* 132: 476–490, 2020. doi:10.1097/ALN.0000000000003062.
46. **Sophocleous L**, **Frerichs I**, **Miedema M**, **Kallio M**, **Papadouri T**, **Karaoli C**, **Becher T**, **Tingay DG**, **van Kaam AH**, **Bayford R**, **Waldmann AD.** Clinical performance of a novel textile interface for neonatal chest electrical impedance tomography. *Physiol Meas* 39: 044004, 2018. doi:10.1088/1361-6579/aab513.
47. **Sophocleous L**, **Waldmann AD**, **Becher T**, **Kallio M**, **Rahtu M**, **Miedema M**, **Papadouri T**, **Karaoli C**, **Tingay DG**, **Van Kaam AH**, **Yerworth R**, **Bayford R**, **Frerichs I.** Effect of sternal electrode gap and belt rotation on the robustness of pulmonary electrical impedance tomography parameters. *Physiol Meas* 41: 035003, 2020. doi:10.1088/1361-6579/ab7b42.
48. **Spadaro S**, **Mauri T**, **Böhm SH**, **Scaramuzzo G**, **Turrini C**, **Waldmann AD**, **Ragazzi R**, **Pesenti A**, **Volta CA.** Variation of poorly ventilated lung units (silent spaces) measured by electrical impedance tomography to dynamically assess recruitment. *Crit Care* 22: 26, 2018. doi:10.1186/s13054-017-1931-7.
49. **Thürk F**, **Elenkov M**, **Waldmann AD**, **Böhme S**, **Braun C**, **Adler A**, **Kaniusas E.** Influence of reconstruction settings in electrical impedance tomography on figures of merit and physiological parameters. *Physiol Meas* 40: 094003, 2019. doi:10.1088/1361-6579/ab248e.
50. **Tusman G**, **Sipmann FS**, **Bohm SH.** Rationale of dead space measurement by volumetric capnography. *Anesth Analg* 114: 866–874, 2012. doi:10.1213/ANE.0b013e318247f6cc.
51. **Ukere A**, **März A**, **Wodack KH**, **Trepte CJ**, **Haese A**, **Waldmann AD**, **Böhm SH**, **Reuter DA.** Perioperative assessment of regional ventilation during changing body positions and ventilation conditions by electrical impedance tomography. *Br J Anaesth* 117: 228–235, 2016. doi:10.1093/bja/aew188.
52. **Vogt B**, **Pulletz S**, **Elke G**, **Zhao Z**, **Zabel P**, **Weiler N**, **Frerichs I.** Spatial and temporal heterogeneity of regional lung ventilation determined by electrical impedance tomography during pulmonary function testing. *J Appl Physiol (1985)* 113: 1154–1161, 2012. doi:10.1152/japplphysiol.01630.2011.
53. **Vonk Noordegraaf A**, **Kunst PW**, **Janse A**, **Marcus JT**, **Postmus PE**, **Faes TJ**, **de Vries PM.** Pulmonary perfusion measured by means of electrical impedance tomography. *Physiol Meas* 19: 263–273, 1998. doi:10.1088/0967-3334/19/2/013.
54. **Waldmann AD**, **Böhm S**, **Mosing M**, **Tusman G.** Distribution of regional peak expiratory flow under different body positions and ventilation conditions determined by electrical impedance tomography (EIT). In: *15 Kongress der Deutschen interdisziplinären Vereinigung für Intensiv- und Notfallmedizin*. Leipzig, Germany: Deutsche interdisziplinären Vereinigung für Intensiv- und Notfallmedizin, 2015.